Quantitative Electron Diffraction Data of Amorphous Materials

Jürgen Ankele[a], Joachim Mayer[b], Peter Lamparter[c], and Siegfried Steeb[c]

[a] Alcatel SEL AG, Lorenzstraße 10, D-70435 Stuttgart, Germany
[b] Rheinisch-Westfälische Technische Hochschule Aachen, Gemeinschaftslabor für Elektronenmikroskopie, Ahornstraße 55, D-52074 Aachen, Germany
[c] Max-Planck-Institut für Metallforschung, Heisenbergstraße 3, D-70569 Stuttgart, Germany

Reprint requests to Dr. P. L.; Fax: +49 (0)711 689-3312; E-mail: Lamparter@mf.mpg.de

Z. Naturforsch. **60a,** 459 – 468 (2005); received March 15, 2005

A method has been developed to obtain quantitative electron diffraction data up to a value of $Q = 20$ Å^{-1} of the modulus of the scattering vector. The experiments were performed on a commercially available transmission electron microscope equipped with a so-called omega energy filter. An analytical multiple scattering correction was applied. The electron diffraction results obtained with amorphous germanium were compared with X-ray and neutron diffraction data and showed good agreement. For an amorphous $Ni_{63}Nb_{37}$ sample it was shown that it is possible to estimate the multiple scattering intensity without exact knowledge of the sample thickness. This technique was applied to derive the structure factor for electron diffraction of two precursor-derived amorphous Si-C-N ceramics (a-$Si_{24}C_{43}N_{33}$ and a-$Si_{40}C_{24}N_{36}$). The results are consistent with corresponding X-ray diffraction data and with an existing structural model for such ceramics.

Key words: Electron Diffraction; Amorphous Materials; Multiple Scattering Correction.

1. Introduction

In the study of amorphous materials, quantitative electron diffraction experiments may be superior to the competing neutron and X-ray diffraction techniques for a number of reasons:

i) For thin amorphous films electron diffraction is often the only possibility to obtain sufficient intensity for the evaluation of structural information;

ii) in case of samples consisting of more than one phase (e. g., a crystalline and an amorphous phase) the use of a transmission electron microscope makes it possible to perform selected area diffraction using a finely focused beam;

iii) for amorphous phases consisting of two or more chemical elements, electron diffraction is an additional experiment, besides X-ray and neutron diffraction, which increases the information about the partial structure factors of the sample (the so-called contrast variation method).

In the past much effort has been devoted to perform electron diffraction experiments with amorphous specimens (see, for instance, [1 – 3]). The problems associated with the evaluation of quantitative diffraction data, as given by the coherently diffracted intensity in absolute units, are due to the strong Coulomb interaction between the beam electrons and the atoms of the sample. This causes strong inelastic and multiple scattering contributions. During the last years several well designed energy filters became available and were used for electron diffraction with amorphous samples [4 – 6]. Applying these energy filters, almost exclusively the elastically scattered intensity is recorded, which provides the basis for the evaluation of structural data. We also use an analytical multiple scattering theory to correct the measured diffraction data for the multiple scattering effect.

In the present work, based on our previous work on quantitative electron diffraction with amorphous specimens [7, 8], we proceed to thinner samples, improve the data treatment and reach higher values of the modulus Q of the scattering vector by combining several CCD-camera images. We have developed a reliability test for the applied method for multiple scattering correction, and we have performed X-ray and neutron diffraction experiments with amorphous (a)-Ge to compare these data with the electron diffraction result. This comparison provides a critical test because in case of a single component amorphous sample identical structure factors have to be obtained with the three types of radiation.

We apply this electron diffraction method to amorphous (a)-$Ni_{63}Nb_{37}$ as an example for a sample with unknown or variable thickness which is the normal case for conventionally thinned TEM samples. As the partial structure factors for this material are known [9] the total structure factor, as expected for electron diffraction, can be predicted and thus the multiple scattering correction can be tested for this kind of samples.

Finally, we present electron and X-ray diffraction results for two amorphous Si-C-N precursor ceramics and discuss our results in the framework of existing structural models.

Details of the following description of the theoretical background and the experimental work can be found in [10].

2. Theoretical Background

2.1. Inelastically Scattered Electrons

The scattered intensity of an electron diffraction experiment can be subdivided in elastically coherently scattered intensity and in inelastically scattered intensity. Inelastically scattered intensity can be coherent or incoherent and occurs when the scattered electron looses energy by plasmon or inner shell excitation, electron-Compton or thermal diffuse scattering (for details see [11]). Since the omega energy filter allows only electrons with an energy loss of $\Delta E < 5$ eV to pass (see below), besides the elastically scattered intensity only thermal diffuse scattering (with an energy loss of about 0.03 eV), and at low diffraction angles ($Q < 1.5$ Å^{-1}) a small fraction of the electron-Compton scattering intensity reaches the electron detector.

2.2. Coherently Elastically Scattered Electrons

The total structure factor $S(Q)$, which contains the structural information, is calculated according to Faber and Ziman [12] from the normalized coherently scattered intensity per atom I_{coh}:

$$S(Q) = \frac{I_{\mathrm{coh}}(Q) - \left(\langle f^2\rangle - \langle f\rangle^2\right)}{\langle f\rangle^2}, \tag{1}$$

where

$$Q = \frac{4\pi \sin\Theta}{\lambda}, \quad \langle f^2\rangle = \sum_{i=1}^{M} c_i f_i^2, \quad \langle f\rangle = \sum_{i=1}^{M} c_i f_i,$$

Q = modulus of the scattering vector, 2Θ = scattering angle, λ = wavelength, $f_i(Q)$ = atomic scattering factor or scattering length of element i, c_i = atomic concentration of element i, M = number of elements in the sample.

The normalization factor that leads from the measured intensity to I_{coh} depends on the experimental parameters, such as primary intensity, detector sensitivity, transmission function of the energy filter, and can be determined with the formalisms of Krogh-Moe [13] or Gingrich [14].

If the sample contains more than one element ($M > 1$), the total structure factor is the weighted sum of $M(M+1)/2$ partial structure factors $S_{ij}(Q)$ $(= S_{ji}(Q))$:

$$\begin{aligned} S(Q) &= \langle f\rangle^{-2} \sum_{i=1}^{M}\sum_{j=1}^{M} c_i c_j f_i f_j S_{ij}(Q) \\ &= \sum_{i=1}^{M}\sum_{j=1}^{M} W_{ij} S_{ij}(Q). \end{aligned} \tag{2}$$

The weighting factors $W_{ij} = c_i c_j f_i f_j / \langle f\rangle^2$ depend on the type of radiation used.

The total pair correlation function $G(R)$ is related to the structure factor by a Fourier transformation:

$$\begin{aligned} G(R) &= 4\pi R(\rho(R) - \rho_0) \\ &= \frac{2}{\pi}\int_0^{\infty} (S(Q)-1) Q \sin(QR)\,\mathrm{d}Q, \end{aligned} \tag{3}$$

where $\rho(R)$ = local atomic number density at distance R from a reference atom at $R = 0$, ρ_0 = average atomic number density. This relation also applies to the partial functions $G_{ij}(R)$ and $S_{ij}(Q)$ (where $\rho(R)$ has to be replaced by $\rho_{ij}(R)/c_j$).

The coordination numbers Z_{ij} (j around i) are given by the areas below the peaks of the partial radial distribution functions $4\pi R^2 \rho_{ij}(R)$. If a peak in the total pair correlation function belongs to only one correlation ij, it is possible to calculate Z_{ij} directly from the total function without knowledge of the partial functions (taking the weight of the partial function into account by the factor c_j/W_{ij}).

2.3. Multiple Scattering Correction

The ideas for the analytical multiple scattering correction that are presented in this chapter are based on

the work of Gjønnes [15], Anstis et al. [16], and mainly Egerton [11]. The premises are:

1. Only elastically scattered intensity is taken into account.
2. The sample geometry is flat.
3. Only statistically independent scattering events happen; that is, a mean free path for elastic scattering λ_{mf} can be defined.
4. Only small scattering angles occur, i. e., (Q-dependent) absorption needs not to be considered.

For thin sputtered films and a 120 kV electron microscope ($\Theta = 3.0^\circ$ for $Q = 20$ Å^{-1}) these premises are fulfilled.

The relationships between non-scattered electrons, $I_0(D)$, electrons that undergo one scattering event, $I_1(D)$, electrons that undergo two scattering events, $I_2(D)$, ect., are described by the Poisson distribution (with respect to D):

$$I_k(D) = \frac{I_\mathrm{e}}{k!}(D/\lambda_{\mathrm{mf}})^k \exp(-D/\lambda_{\mathrm{mf}}), \tag{4}$$

where D is the sample thickness and I_e is the intensity of the incident electrons. $I_k(D, \overrightarrow{Q})$ can be decomposed into this D-dependent intensity term $I_k(D)$ and a normalized Q-dependent distribution term $P_k(\overrightarrow{Q})$:

$$\begin{aligned} &I_k(D, \overrightarrow{Q}) = I_k(D) \cdot P_k(\overrightarrow{Q}), \\ &\text{with } \int P_k(\overrightarrow{Q})\mathrm{d}Q = 1. \end{aligned} \tag{5}$$

With $P_{k+1}(\overrightarrow{Q}) = P_k(\overrightarrow{Q}) * P_k(\overrightarrow{Q})$ and $*$ denoting the two-dimensional convolution, the scattered intensity can be described by the equation

$$\begin{aligned} I(D, \overrightarrow{Q}) = I_0(D)\Bigg[&\delta(\overrightarrow{Q}) + \frac{D}{\lambda_{\mathrm{mf}}} P_1(\overrightarrow{Q}) + \frac{1}{2!}\left(\frac{D}{\lambda_{\mathrm{mf}}}\right)^2 P_1(\overrightarrow{Q}) * P_1(\overrightarrow{Q}) \\ &+ \frac{1}{3!}\left(\frac{D}{\lambda_{\mathrm{mf}}}\right)^3 e^{-\frac{D}{\lambda_{\mathrm{mf}}}} P_1(\overrightarrow{Q}) * P_1(\overrightarrow{Q}) * P_1(\overrightarrow{Q}) + \ldots\Bigg]. \end{aligned} \tag{6}$$

Since amorphous specimens show diffuse diffraction rings, i. e., diffraction patterns with rotational symmetry, the one-dimensional radial intensity function $I^\mathrm{r}(D,Q)$ can be used to perform the deconvolution of (6), using the Hankel transformation [17]:

$$\tilde{I}^\mathrm{r}(D,R) = \frac{1}{2\pi}\int_0^\infty I^\mathrm{r}(D,Q) Q J_0(QR)\mathrm{d}Q, \tag{7a}$$

$$I^\mathrm{r}(D,Q) = 2\pi\int_0^\infty \tilde{I}^\mathrm{r}(D,R) R J_0(QR)\mathrm{d}R, \tag{7b}$$

where $J_0(QR)$ is the zero order Bessel function. This leads to the correction formula for multiple scattering

$$\tilde{I}_1^\mathrm{r}(D,R) = I_0(D)\ln(\tilde{I}^\mathrm{r}(D,R)/I_0(D)). \tag{8}$$

$I^\mathrm{r}(D,Q)$ is then obtained from (7b). The non-scattered intensity $I_0(D)$ in (8) cannot be detected with our experimental set up, because the dynamical range of the CCD-camera was limited to 16,384 counts/pixel, and a beamstop for small scattering angles was used. The modified correction formula takes this into account:

$$\tilde{I}_1^\mathrm{r}(D,Q) = \frac{I_{\mathrm{tot}}(D)}{\mathrm{e}^{D/\lambda_{\mathrm{mf}}} - 1} \ln\left(\frac{\tilde{I}^\mathrm{r}(D,R)(\mathrm{e}^{D/\lambda_{\mathrm{mf}}} - 1)}{I_{\mathrm{tot}}(D)} + 1\right). \tag{9}$$

The quantity $I_{\mathrm{tot}}(D) = I_1(D) + I_2(D) + I_3(D) + \ldots$ can be calculated from the experimentally measured $I^\mathrm{r}(D,Q)$:

$$I_{\mathrm{tot}}(D) = \int_{Q_{\min}}^{Q_{\max}} 2\pi Q I^\mathrm{r}(D,Q)\mathrm{d}Q. \tag{10}$$

To obtain a reliable value for $I_{\mathrm{tot}}(D)$ and to minimize truncation effects in the Hankel transformation, the experimentally measured $I^\mathrm{r}(D,Q)$ was extended to the range 20 Å$^{-1} < Q < 50$ Å^{-1} using the run of the function $\langle f^2(Q)\rangle$.

The ratio D/λ_{mf}, with $\lambda_{\mathrm{mf}} = 1/(\rho_0\sigma_{\mathrm{el}})$, is essential for the correction for multiple scattering, where σ_{el} is the total cross section for elastically scattered electrons. Values of σ_{el} were calculated by Riley et al. [18]. If the sample thickness D and the density ρ_0 of sputtered samples are known, e.g., in case of thin films determined independently from an X-ray reflectivity experiment [19, 20], no adjustable variables have to be used for the multiple scattering correction.

From the measured (and corrected) intensity $I^\mathrm{r}(D_2,Q)$ of a sample with thickness D_2 the scattered intensity $I^\mathrm{r}(D_1,Q)$ for any thickness D_1 and the same incident intensity I_e can be calculated using the expression

$$\tilde{I}_1^{\mathrm{r}}(D,R) = \left[\left(\frac{\tilde{I}^{\mathrm{r}}(D_2,R)(\mathrm{e}^{D_2/\lambda_{\mathrm{mf}}}-1)}{I_{\mathrm{tot}}(D_2)}+1\right)^{\frac{D_1}{D_2}\mathrm{e}^{(D_1-D_2)/\lambda_{\mathrm{mf}}}} - 1\right]\frac{I_{\mathrm{tot}}(D)}{\mathrm{e}^{D_1/\lambda_{\mathrm{mf}}}-1}. \tag{11}$$

With this relation it is possible to check the multiple scattering correction experimentally.

3. Experimental

3.1. Sample Preparation

Amorphous germanium samples with different thicknesses, appropriate for performing electron, X-ray and neutron diffraction experiments, were produced within an rf-sputtering device (Leybold-Heraeus, model Z400). The growth conditions were the same for all samples. This is an important condition for a meaningful comparison of the results of the three different diffraction experiments. During the sputtering process the substrates were kept at room temperature with a cooling water circuit.

The a-Ge film for the electron diffraction experiment was sputtered onto a freshly cleaved rocksalt substrate. The substrate was removed with de-ionized water and the a-Ge film was collected on a copper grid with 1,500 mesh/inch, which then is used as sample holder in the electron microscope. The thickness and density of the a-Ge film were determined independently by an X-ray reflectivity measurement [19, 20]. For this, a second Ge film was deposited onto a SiO_2 substrate at the same time as the film on the rocksalt substrate. The a-Ge sample for the X-ray diffraction experiment was sputtered onto a 5 μm thick mylar foil. The sample thickness of 30 μm, measured with a mechanical probe, was about half of the optimum thickness ($1/e$ transmission), i.e. no substantial X-ray multiple scattering occurred. For the neutron diffraction sample an Al foil was used as substrate. The Al foil was removed with an NaOH-water solution, and the remaining a-Ge powder (1.12 g) was filled into a vanadium cylinder as sample holder. The density of the sputtered a-Ge material, measured with the Archimedean method, was 5.33 g/cm^3.

Amorphous $Ni_{63}Nb_{37}$ ribbons with a thickness of about 10 μm were produced by melt-spinning [9]. These ribbons can be directly used for the X-ray diffraction experiment. For the electron diffraction experiment, a piece of ribbon was dimpled and then ion-thinned until a small hole appeared. At the edge of this hole, the sample is thin enough for electron diffraction.

The a-$Si_{40}C_{24}N_{36}$ and a-$Si_{24}C_{43}N_{33}$ samples were produced with the precursor technique. A detailed description can be found in [21, 22] for a-$Si_{40}C_{24}N_{36}$ and in [23, 24] for a-$Si_{24}C_{43}N_{33}$. For the X-ray diffraction experiment an a-$Si_{40}C_{24}N_{36}$ sample of 0.8 mm thickness and a-$Si_{24}C_{43}N_{33}$ powder were used. For electron diffraction the samples were prepared in the same way as a-$Ni_{63}Nb_{37}$.

3.2. Diffraction Experiments

Electron Diffraction

The electron diffraction experiments were performed in a transmission electron microscope Zeiss EM 912 Omega, equipped with an omega energy filter [25] and a Gatan slow scan CCD-camera with 1024×1024 pixels as detector. The wavelength of the electrons was $\lambda = 0.00335$ Å. The omega energy filter was an imaging magnetostatic energy filter which corrects imaging aberrations up to the second order. In principle it is possible to work with an energy resolution of about $\Delta E = \pm 1$ eV. But with this value the transmission function of the energy filter is not constant and intensity variations on the amorphous diffraction rings occurred. Therefore a value of $\Delta E = \pm 5$ eV was chosen because with this value the transmission function of the energy filter is constant over the measured area and the energy resolution is sufficient to filter out plasmon scattered electrons occurring at about $\Delta E \geq 10$ eV.

For calibration of the lateral measurement positions on the area of the CCD-camera and conversion into units of the modulus of the scattering vector Q, the Bragg reflections from a crystalline Si standard were used. Along the diagonal of the CCD-camera the diffracted intensity can be detected up to $Q = 12$ Å^{-1}. To overcome this limitation, additional diffraction images were detected by tilting the incident beam above the sample in order to shift the diffraction image over the CCD-camera. This strategy has the advantage that the measured angular range of scattered intensity is centred on the optical axis of the microscope, and that no conflicts with the transmission function of the energy filter occur.

Normally three (one non-shifted and two shifted) images with an overlap of about 4 Å^{-1} were measured to cover the diffraction range 0 $\text{Å}^{-1} < Q < 20$ Å^{-1}. The exposure time for each image was optimised to make full use of the dynamic range of the CCD-camera of 16,384 counts/pixel, and was in the range of a few to 100 seconds.

In a first step of the data treatment, corrections for the influences of the CCD-camera were performed: the background intensity was measured with closed shutter and subtracted from the diffracted intensity, the effect that the detector pixels have different efficiency was corrected for (gain correction), and a deconvolution with the point spread function (psf) [26, 27] was applied. For the non-shifted images the centre of the diffraction rings was determined and the diffraction rings were radially averaged to obtain the radial profile. For the shifted images a radial line profile from an average over a width of about 100 pixels was obtained. Finally, the profiles of the non-shifted and the shifted images were combined to receive the $I^{\mathrm{r}}(D,Q)$ function.

X-Ray Diffraction

The X-ray diffraction experiments were performed in transmission on a Siemens diffractometer of type F equipped with an Ag-anode ($\lambda = 0.561$ Å) and an Si(Li)-detector with an energy resolution of about 300 eV. The measured intensity was corrected for background, polarization, and absorption [28]. The inelastic (Compton) scattering data were taken from Hubbell et al. [29], and the anomalous diffraction data from Waseda [30]. A multiple scattering correction for X-ray diffraction was not necessary, because the multiple scattering intensity is below 1% of the total scattered intensity for all measured samples.

Neutron Diffraction

The neutron diffraction experiment on a-Ge was performed at the instrument 7C2 of the Laboratoire Léon Brillouin, Saclay. The neutron wavelength was $\lambda = 0.7$ Å. The measured intensity was corrected for background and absorption [31], inelastic scattering [32, 33] and multiple scattering [34]. An additional Q-dependent inelastic scattering contribution, caused by a small amount of hydrogen in the sample, was corrected by Fourier-filtering (for details see [10]).

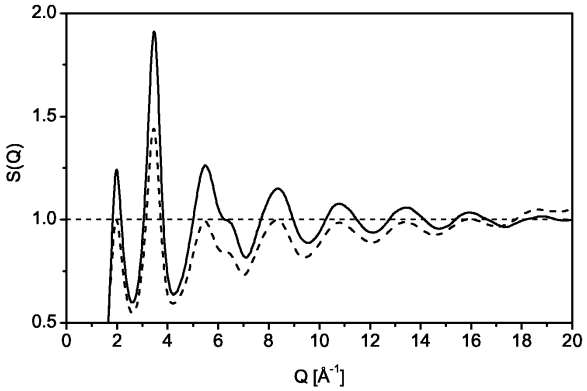

Fig. 1. Structure factor $S(Q)$ of amorphous germanium from electron diffraction with a 72 Å thick film; - - - without multiple scattering correction; — corrected for multiple scattering.

4. Results and Discussion

4.1. Amorphous Germanium

Multiple Scattering Correction for Electron Diffraction with a-Ge

Figure 1 shows the influence of multiple scattering on the structure factor $S(Q)$ for electron diffraction. The thickness of the measured a-Ge sample was 72 Å. Although the ratio $D/\lambda_{\mathrm{mf}} \approx 0.2$ is rather small, the amount of multiple scattering of about 10% is considerable. The necessity for a multiple scattering correction for this kind of experiment is evident: the uncorrected $S(Q)$ (dashed line) decreases with decreasing Q-values, while the corrected $S(Q)$ (solid line) oscillates properly around a value of one and the amplitudes of the oscillations are larger. Generally, the smaller amplitudes of structure factors, if no correction for multiple scattering is applied, lead to smaller amplitudes also in the pair correlation functions and thus to coordination numbers smaller than the real ones.

Sometimes a crack in the thin a-Ge sample occurred and part of the thin foil was folded by 180° to create a double layer at this position. Thus within the sample area two positions with thicknesses D_1 and $D_2 = 2D_1$ can be found. Electron diffraction under the same measuring conditions at these two positions can be used to test the relation (11), i. e., the formalism applied for the multiple scattering correction, on which (11) is based. The measured structure factors $S_1(Q)$ (- - -) of the monolayer ($D_1 = 72$ Å) and $S_2(Q)$ (- · -) of the doublelayer ($D_2 = 144$ Å), both without correction for multiple scattering, are plotted in Figure 2. Then $S_2(Q)$ was transformed, using (11), to a structure factor

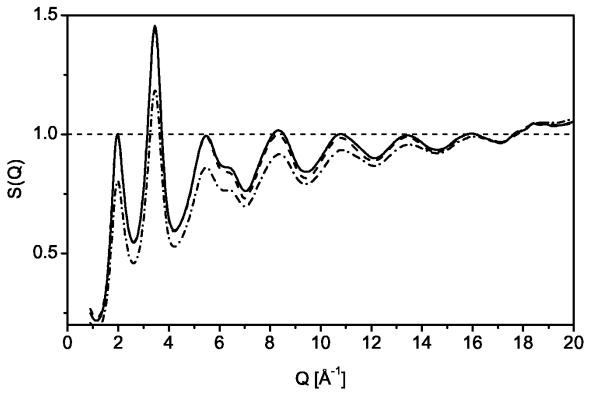

Fig. 2. Test of the multiple scattering formalism for electron diffraction. $S(Q)$ of amorphous germanium with different thickness; - - $D_1 = 72$ Å, measured (same curve as in Fig. 1); - · - $D_2 = 2D_1 = 144$ Å, measured; — calculated for thickness D_1 using the measured data for D_2 as input for (11).

$S_{2\to1}(Q)$ (—) as it would be expected for the thickness D_1. We note that the agreement between the measured $S_1(Q)$ and the calculated $S_{2\to1}(Q)$ is very good. This shows that:

i) the analytical multiple scattering correction works well;

ii) the measured values for the sample thickness D and density ρ_0 as well as the used value for σ_{el} are correct;

iii) with the correction formalism described in chapter 2.3 the coherently scattered intensity is obtained, i. e., no additional intensity has to be taken into account.

Electron, X-Ray and Neutron Diffraction with a-Ge

In Fig. 3 the structure factors $S(Q)$ of a-Ge for electron, X-ray and neutron diffraction, respectively, are presented. The comparison shows very good agreement between the three data sets; no systematic deviations in phase or amplitude are visible. The differences between the electron diffraction result and the X-ray or neutron diffraction result are not larger than the differences between the X-ray and neutron diffraction data. This is a substantial improvement of results of our previous work [7, 8] where the Q-value was limited to $Q = 10$ Å^{-1}, and where we compared the electron diffraction result only with the literature results for X-ray and neutron diffraction experiments which were obtained with a-Ge samples prepared by different procedures.

Table 1. Mean distances R and coordination numbers Z of amorphous germanium, as determined in the present work, and comparison with data from the literature.

Coordination sphere	Electron diffraction		X-Ray diffraction		Neutron diffraction	
	R [Å]	Z	R [Å]	Z	R [Å]	Z
1	2.45	3.7	2.45	3.7	2.46	3.8
	2.45[a]	≈ 4[a]	2.47[b]	3.8[b]	2.46[c]	3.7[c]
2	3.96	17.5	3.93	17.3	3.91	17.4
	4.0[a]	≈ 12[a]	4.0[b]	12.3[b]	4.0[c]	12.1[c]
3	4.94	5.6	4.83	5.2	5.01	7.8
	4.85[a]	≈ 7[a]	4.7[b]	5.5[b]	–	–
4	6.0	27	5.98	28	5.95	27
	5.9[a]	–	6.0[b]	–	6.03[b]	–

[a] [35]; [b] [36]; [c] [37].

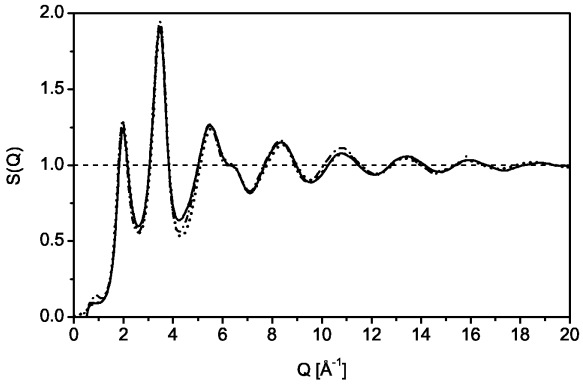

Fig. 3. Structure factor $S(Q)$ of amorphous germanium; — electron diffraction; ··· X-ray diffraction; -·- neutron diffraction.

The mean distances and coordination numbers were determined from the correlation functions $G(R)$, corresponding to $S(Q)$ in Fig. 3, as derived from the three diffraction experiments, and are compiled in Table 1 together with results from the literature. The values for the mean distances and the values of the first two coordination numbers, as obtained in the present work with the three types of radiation, show very good agreement. For the higher coordination spheres the differences are larger, caused by the overlap between the peaks of the higher spheres in $G(R)$, that leads to uncertainties in the integration limits.

4.2. Amorphous $Ni_{63}Nb_{37}$

The partial structure factors of a-$Ni_{63}Nb_{37}$ are known from neutron diffraction experiments with isotopic substitution [9]. With (2) and (3) the total pair correlation function as expected for electron diffraction, $G^{cal}(R)$, can be calculated. Since the value of the sample thickness D is unknown in the electron diffrac-

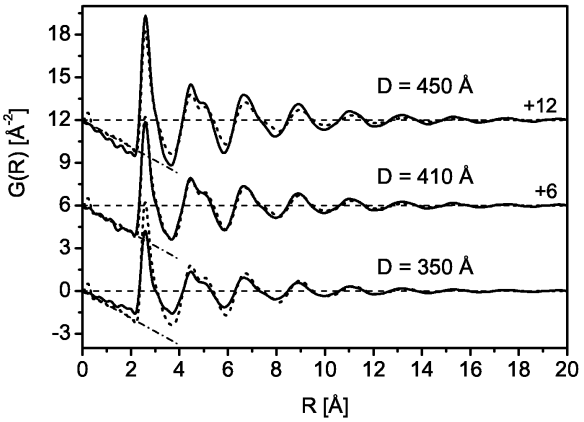

Fig. 4. Total pair correlation functions $G(R)$ of amorphous $Ni_{63}Nb_{37}$; — from electron diffraction using different values for the thickness D (as indicated in the figure) and $\lambda_{mf} =$ 190 Å for the multiple scattering correction; - - - calculated from the partial structure factors from [9] (same curve in the three plots); -·- line $G(R) = -4\pi\rho_0 R$, corresponding to $\rho(R) = 0$.

tion experiment, the multiple scattering correction was performed with a variation of D (using 8.95 g/cm^3 for the density and $\lambda_{mf} = 190$ Å) until the experimentally obtained $G^{exp}(R)$ agreed best with the one calculated from the partial structure factors. Thus, a value of $D = 410$ Åwas found for this sample.

Figure 4 shows $G^{cal}(R)$ (dashed line) and $G^{exp}(R)$ for 410 Å specimen thickness (solid line in the middle), which agree very well with each other. The additionally shown $G^{exp}(R)$ curves for $D = 350$ Å and 450 Å indicate the influence of the D value: a variation of about 10% of the thickness leads to a $G(R)$ with substantial differences in the amplitude.

Another feature can be seen in the region of $R < 2$ Å, where no nearest neighbours occur: as a criterion to find the unknown D value without the knowledge of the partial structure factors, which is the normal case, the line $G(R) = -4\pi\rho_0 R$ at low R-values, corresponding to $\rho(R) = 0$ [cf. (3)], can be used. $G(R)$ for $D = 410$ Å oscillates around the $-4\pi\rho_0 R$ line, while $G(R)$ for $D =$ 350 Å is above and for $D = 450$ Å is below this line. The small oscillations in the range $R < 2$ Å are caused by truncation effects during the Fourier transformation, and by residual (long wavelength-) errors in $S(Q)$.

The electron diffraction experiment on a-$Ni_{63}Nb_{37}$ shows that:

i) the analytical multiple scattering correction can be applied successfully even if D is more than twice the value of λ_{mf};

ii) the oscillations of $G(R)$ around the $-4\pi\rho_0 R$ line can be used as a criterion for the reliability of the multiple scattering correction for samples with unknown thickness.

4.3. Electron and X-Ray Diffraction with a-$Si_{24}C_{43}N_{33}$ and a-$Si_{40}C_{24}N_{36}$

Electron diffraction experiments with a-$Si_{24}C_{43}N_{33}$ and a-$Si_{40}C_{24}N_{36}$ were performed, and the multiple scattering correction was done in the same manner as described in chapter 4.2. We found for a-$Si_{24}C_{43}N_{33}$ (using $\rho_0 = 0.0670$ Å^{-3} and $\lambda_{mf} = 1363$ Å) $D = 900$ Å, and for a-$Si_{40}C_{24}N_{36}$ (using $\rho_0 = 0.0713$ Å^{-3} and $\lambda_{mf} = 1191$ Å) $D = 650$ Å.

Figure 5 shows the obtained structure factors, and Fig. 6 the total pair correlation functions of both samples for electron and X-ray diffraction. In contrast to the element Ge (chapter 4.1), in the present case of a ternary alloy the total structure factors obtained with electrons and X-rays, respectively, must be different, due to the different weights of the partial structure factors in (2). The differences between the electron and X-ray diffraction results are larger for a-$Si_{24}C_{43}N_{33}$ than

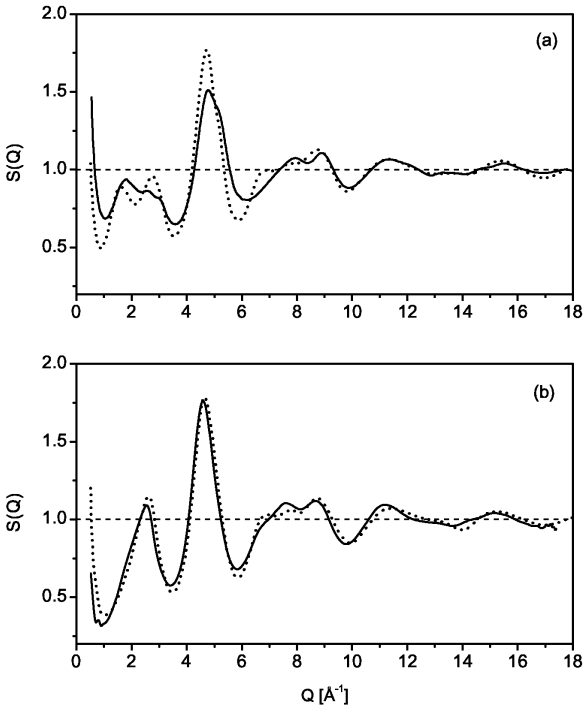

Fig. 5. Structure factors $S(Q)$ of amorphous $Si_{24}C_{43}N_{33}$ (a) and $Si_{40}C_{24}N_{36}$ (b); — from electron diffraction; - - - from X-ray diffraction.

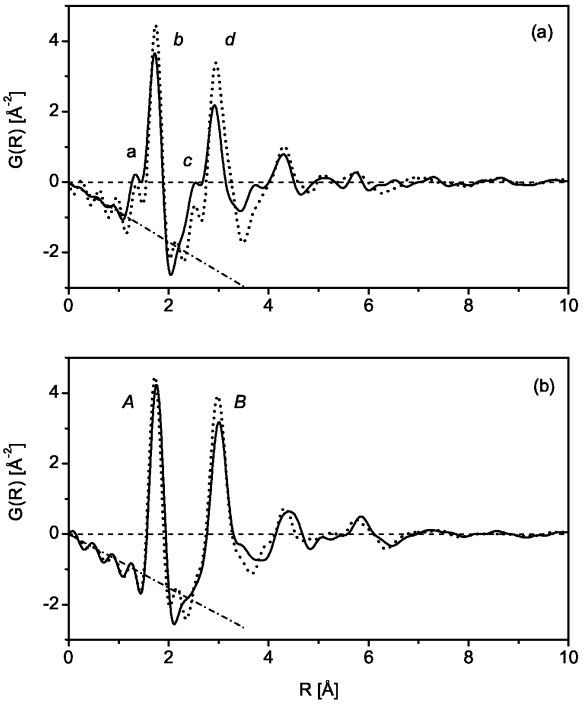

Fig. 6. Total pair correlation functions $G(R)$ of amorphous $Si_{24}C_{43}N_{33}$ (a) and $Si_{40}C_{24}N_{36}$ (b); — from electron diffraction; - - - from X-ray diffraction.

for a-$Si_{40}C_{24}N_{36}$.

Small and wide angle X-ray and neutron diffraction experiments with a-$Si_{24}C_{43}N_{33}$ by Dürr et al. [24, 38, 39] showed that no direct (covalent) Si,Si-, N,N- and Si,C-correlations occur in this ceramic. Together with the fact that the Si/N concentration relation is $c_{Si}/c_N = 3/4$, Dürr et al. proposed the following model for a-$Si_{24}C_{43}N_{33}$: SiN_4 tetrahedra, as structural units, are linked together in amorphous Si_3N_4 regions with short range order similar to crystalline α-Si_3N_4. These regions are dispersed in a matrix of amorphous graphite-like carbon. In the following, we will use this model to interpret the present diffraction results, taking into consideration the obtained differences between the electron and X-ray diffraction results.

First, we compare the atomic distances in α-Si_3N_4 and graphite with the peak positions of the $G(R)$ functions shown in Fig. 6a: The small peaks labelled as *a* ($R^x = 1.35$ Å, $R^e = 1.33$ Å) and *c* ($R^x = 2.52$ Å, $R^e = 2.54$ Å) belong to C,C-correlations (graphite: $R_{CC} = 1.42$ Å and 2.46 Å). The peak *b* ($R^x = 1.74$ Å, $R^e = 1.72$ Å) corresponds to the Si,N-correlation (α-Si_3N_4: $R_{SiN} = 1.76$ Å), and for the peak *d* ($R^x = 2.94$ Å, $R^e = 2.92$ Å) Si,Si- and N,N-correlations have to be considered (α-Si_3N_4: $R_{SiSi} = 2.72 - 2.97$ Å, $R_{NN} = 2.81$ and 2.94 Å).

For the determination of coordination numbers the peaks occuring in the correlation functions $\rho(R)$ were fitted by Gaussians. From the area of peak *b*, using the appropriate weighting factors W_{ij}, the coordination number $Z_{SiN} = 3.7$ (corresponding to $Z_{NSi} = c_{Si}/c_N Z_{SiN} = 2.7$) was obtained both with X-rays and electrons. This agreement shows that the methods for quantitative electron diffraction, as applied in the present paper, are reliable. For the evaluation of peak *d* the diffraction contrast between X-rays and electrons can be used. Due to the different weights W_{ij} of the Si,Si and the N,N contributions in (2) for the two types of radiation also the areas below the peak *d* are different. This provides two equations for the determination of the coordination numbers with the result: $Z_{SiSi} = 5.5$ and $Z_{NN} = 8.6$. These values presented upper limits because small amounts of Si,C-, N,C- and C,C-correlations may also contribute to the peak *d*. The peaks *a* and *c* are too small for an accurate calculation of the coordination numbers. Altogether, the measured electron and X-ray diffraction data agree with the proposed model for a-$Si_{24}C_{43}N_{33}$.

The $G(R)$ functions of a-$Si_{40}C_{24}N_{36}$ (Fig. 6b) exhibit two peaks *A* ($R^x = 1.73$ Å and $R^e = 1.76$ Å) and *B* ($R^x = 2.98$ Å and $R^e = 3.01$ Å), which correspond to the peaks *c* and *d* of a-$Si_{40}C_{24}N_{36}$ (Fig. 6a), whereas no peaks belonging to C,C-correlations are detected. The a-$Si_{40}C_{24}N_{36}$ ceramic contains less carbon and, because of the higher Si content (corresponding to the relation $c_{Si}/c_N = 1.1 > 3/4$), part of the C atoms (17 at% out of 24 at%) is bonded in mixed $Si(C,N)_4$ tetrahedra, forming an amorphous $Si_3(C,N)_4$ phase [40, 41]. Hence the amount of free carbon (7 at% out of 24 at%), forming a graphite-like amorphous carbon phase, is smaller by a factor of 6 than in the a-$Si_{24}C_{43}N_{33}$ ceramic, and thus too small to cause detectable peaks in the $G(R)$ functions.

Treating the elements N and C as a single component X (and using a properly averaged scattering length), the Si coordination in the SiX_4 units can be calculated from the peak *A* in Figure 6b. The agreement of the values $Z_{SiX} = 3.6$ (from electron diffraction) and $Z_{SiX} = 3.5$ (from X-ray diffraction) again shows the reliability of the electron diffraction method.

At the second maximum *B* ($R^x = 2.98$ Å and $R^e = 3.01$ Å) corresponding distances can be found in the

crystalline phases α-Si_3N_4 and c-SiC for all possible correlations. The analysis of the different weighting factors and different areas under the $G(R)$ functions of the two diffraction experiments allowed no clear assignment to one or two correlations and therefore no calculation of Z_{ij}-values for a-$Si_{40}C_{24}N_{36}$. At this point additional diffraction experiments, such as neutron diffraction with isotopic substitution, are necessary in order to obtain partial coordination numbers.

5. Conclusions

Diffraction experiments with amorphous Ge showed that quantitative electron diffraction with amorphous materials, using an imaging energy filter and a multiple scattering correction, can be performed with comparable accuracy as X-ray and neutron diffraction. A prerequisite for an analytical multiple scattering correction is the knowledge of the sample thickness and the density which can be determined for thin films independently by an X-ray reflectivity measurement.

For samples with unknown thickness the reliability of the multiple scattering correction, using the thickness as a free parameter, can be estimated by comparison of the resulting pair correlation function with the theoretical behaviour in the range of distances below the nearest neighbour distance. In this way, reliable electron diffraction results were obtained for an amorphous Ni-Nb alloy, which are consistent with neutron diffraction results.

Electron and X-ray scattering results for amorphous Si-C-N ceramics can be understood with a two phase model consisting of an amorphous Si_3N_4 phase and an amorphous carbon phase.

Acknowledgement

We gratefully acknowledge financial support by the Deutsche Forschungsgemeinschaft.

[1] S. Steeb, Dissertation, Universität Stuttgart, 1958.
[2] J. F. Graczyk and S. C. Moss, Rev. Sci. Instrum. **40**, 424 (1969).
[3] F. Paasche, H. Olbrich, U. Schestag, P. Lamparter, and S. Steeb, Z. Naturforsch. **37a**, 1139 (1982).
[4] D. J. H. Cockayn and D. R. McKenzie, Acta Cryst. A**44**, 870 (1988).
[5] L. Reimer, I. Fromm, and I. Naundorf, Ultramicroscopy **32**, 80 (1990).
[6] L. C. Qin, A. J. Garrett-Reed, and L. W. Hobbs, in: Proc. 50th Annual Meeting of the Electron Microscopy Society of America, San Francisco Press, San Francisco 1992, p. 350.
[7] J. Ankele, J. Mayer, P. Lamparter, and S. Steeb, Z. Naturforsch. **49a**, 771 (1994).
[8] J. Ankele, J. Mayer, P. Lamparter, and S. Steeb, J. Non-Cryst. Solids **192 & 193**, 679 (1995).
[9] P. Lamparter, M. Schaal, and S. Steeb, Inst. Phys. Conf. Ser. No 101 **1**, 51 (1990).
[10] J. Ankele, Dissertation, Universität Stuttgart, 1997.
[11] R. F. Egerton, Electron Energy Loss Spectroscopy in the Microscope, Plenum Press, New York 1986.
[12] T. E. Faber and J. M. Ziman, Philos. Mag. **11**, 153 (1965).
[13] J. Krogh-Moe, Acta Cryst. **9**, 951 (1956).
[14] N. S. Gingrich, Rev. Mod. Phys. **15**, 90 (1943).
[15] J. Gjønnes, Acta Cryst. **12**, 976 (1959).
[16] S. R. Anstis, Z. Liu, and M. Lake, Ultramicroscopy **26**, 65 (1988).
[17] J. S. Walker, Fourier Analysis, Oxford University Press, New York, Oxford 1988, p. 260.
[18] M. E. Riley, C. J. Mac Callum, and F. Biggs, At. Data Nucl. Data Tables **15**, 443 (1975).
[19] F. Stanglmeier, B. Lengeler, W. Weber, H. Göbel, and M. Schuster, Acta Cryst. Sect. A **48**, 626 (1992).
[20] C. Schug, Dissertation, Universität Stuttgart, 1997.
[21] M. Frieß, J. Bill, F. Aldinger, D. V. Szabò, and R. Riedel, Key Eng. Mat. **89 – 91**, 95 (1994).
[22] A. Jalowiecki, Dissertation, Universität Stuttgart, 1997.
[23] A. Kienzle, K. Wurm, J. Bill, F. Aldinger, and R. Riedel, in: Proc. of the Munic Silicon Days, 1. and 2. August 1994: Organosilicon Chemistry II, From Molecules to Materials (Eds. N. Auner and J. Weis), Verlag Chemie, Weinheim 1996, p. 725.
[24] J. Dürr, Dissertation, Universität Stuttgart, 1997.
[25] J. Bihr, G. Benner, D. Krahl, A. Rilk, and E. Weimer, in: Proc. 49th Annual Meeting of the Electron Microscopy Society of America EMSA (Ed. W. Bailey), San Francisco Press, Inc., San Francisco 1991, p. 354.
[26] W. Nüchter, A. L. Weickenmeier, and J. Mayer, Inst. Phys. Conf. Ser. No 147: Sect. 8, 309 (1995).
[27] A. L. Weickenmeier, W. Nüchter, and J. Mayer, Optik **99**, 147 (1995).
[28] C. N. J. Wagner, J. Non-Cryst. Solids **31**, 1 (1978).
[29] J. H. Hubbell, W. J. Veigele, E. A. Briggs, R. T. Brown, D. T. Cromer, and R. J. Howerton, J. Phys. Chem. Ref. Data **4**, 471 (1975).
[30] Y. Waseda, Lect. Notes Phys. **204**, Springer, Berlin 1984, p. 119.
[31] H. H. Paalman and C. J. Pings, J. Appl. Phys. **33**, 2635 (1962).
[32] G. Placzek, Phys. Rev. **31**, 377 (1952).

[33] J. L. Yarnell, M. J. Katz, R. G. Wenzel, and S. H. Koenig, Phys. Rev. A **7**, 2130 (1973).
[34] V. F. Sears, Adv. Phys. **24**, 1 (1975).
[35] J. F. Graczyk and P. Chaudhari, Phys. Status Solidi (b) **58**, 163 (1973).
[36] R. J. Temkin, W. Paul, and G. A. N. Connell, Adv. Phys. **22**, 581 (1973).
[37] G. Etherington, A. C. Wright, T. Wenzel, J. C. Dore, J. H. Clarke, and R. N. Sinclair, J. Non-Cryst. Solids **48**, 265 (1982).
[38] J. Dürr, S. Schempp, P. Lamparter, J. Bill, S. Steeb, and F. Aldinger, Solid State Ionics **101 – 103**, 1041 (1997).
[39] J. Dürr, P. Lamparter, J. Bill, S. Steeb, and F. Aldinger, J. Non-Cryst. Solids **232 – 234**, 155 (1998).
[40] S. Schempp, J. Dürr, P. Lamparter, J. Bill, and F. Aldinger, Z. Naturforsch. **53a**, 127 (1998).
[41] J. Haug, P. Lamparter, M. Weinmann, and F. Aldinger, Chem. Mater. **16**, 72 (2004).